ELSEVIER

Deep-Sea Research II 51 (2004) 3029–3042

DEEP-SEA RESEARCH
PART II

www.elsevier.com/locate/dsr2

An examination of the radiative and dissipative properties of deep ocean internal tides

Louis C. St. Laurent[a,*], Jonathan D. Nash[b]

[a]*Department of Oceanography, Florida State University, Tallahassee, Florida, USA*
[b]*College of Oceanic and Atmospheric Science, Oregon State University, Corvallis, Oregon, USA*

Abstract

In this study, the energy flux and energy dissipation of deep ocean internal tides are examined. Properties of the internal tide from two distinct generation regions are contrasted: the Mid-Atlantic Ridge (MAR) and the Hawaiian Ridge. Considerable differences are noted for the baroclinic energy flux, $\langle \mathbf{u}'p' \rangle$, radiated from each site. Radiation from the MAR is relatively rich in high modes, with an energy flux spectral peak at mode 5 and modes 10 and greater accounting for 40% of the total flux. In contrast, Hawaiian Ridge radiation is dominantly composed of modes 1 and 2, with modes 10 and greater accounting for less than 5% of the total flux. Depth integrated energy flux levels are $O(1)\,\mathrm{kW\,m^{-1}}$ at the MAR site, and $O(10)\mathrm{kW\,m^{-1}}$ at the Hawaiian Ridge. Despite these differences, observed turbulent dissipation rates at these sites are similar in magnitude and depth dependence. Decay scales, estimated as $L_\varepsilon = (\int_{-H}^{0} \mathbf{u}'p'\,\mathrm{d}z)/(\int_{-H}^{0} \rho_0 \varepsilon\,\mathrm{d}z)$, range from $O(100)$km to $O(1000)$ km. The mean decay scale based on the MAR data is 230 km, a factor of 3 smaller than at the Hawaiian Ridge site. We demonstrate that the dissipation level scales with the energy flux available in the high modes, which is comparable at both sites, rather than the total energy flux.

1. Introduction

There is a renewed interest in internal tides, in part due to the improved observations of sea surface elevation by the Topex/Poseidon altimeter. These data have been used to constrain hydrodynamic models of the tides, and hence, produce accurate estimates of open-ocean barotropic tides (Egbert et al., 1994; Egbert, 1997). The residuals of such models have also been analyzed, and Egbert and Ray (2000, 2001) have interpreted patterns of implied barotropic to baroclinic tidal conversion. Specifically, these authors have identified a number of deep ocean regions where barotropic tidal energy is likely being transferred to internal tides.

While the global maps of Egbert and Ray provide insight into the spatial variations of the internal tides, they give no direct means of assessing in situ properties. Such studies require direct measurements from the ocean. While much work has focused on the internal tides generated

*Corresponding author.
E-mail address: lous@ocean.fsu.edu (L.C. St. Laurent).

0967-0645/$ - see front matter © 2004 Elsevier Ltd. All rights reserved.
doi:10.1016/j.dsr2.2004.09.008

on continental shelves, canyons, straits, and fjords; only two prominent deep-ocean internal tide generation sites have been examined in dedicated field programs: the Mid-Atlantic Ridge site of the Brazil Basin Tracer Release Experiment (BBTRE), and the Hawaiian Ridge during the Hawaii Ocean Mixing Experiment (HOME). In the material that follows, we describe observations of internal tide energetics for each of these deep-ocean generation regions. While there are a number of publications describing various aspects of the internal tide at each of these sites, no previous attempt has been made to compare and contrast the measured properties. Such is the purpose of this article.

Numerous studies have addressed the internal tide generation problem. Original work by Cox and Sandstrom (1962), Baines (1973, 1982) and Bell (1975) provided the basis for later work. Further analytic formulations examined the initial transient wave response, finite depth effects, depth-varying stratification, spatial variations in topography and tidal forcing, and wave generation by finite amplitude topography of arbitrary steepness (Hibiya, 1986; St. Laurent and Garrett, 2002; Llewellyn Smith and Young, 2002, 2003; Balmforth et al., 2002; Khatiwala, 2003; St. Laurent et al., 2003; Petrelis et al., 2004). Numerical simulations of internal tide generation have also examined critical and supercritical generation phenomena, nonhydrostatic effects, instability, and mixing (Khatiwala, 2003; Legg and Adcroft, 2003; Legg, 2004a, b; Slinn and Levine, 2003). We neglect here references to the vast literature on coastal, hydraulically controlled, and nonlinear internal tide generation. Instead, the focus of this paper is on deep-ocean internal tides where linear dynamics and low Froude numbers generally characterize the wave generation. Moreover, a detailed discussion of internal tide generation is beyond the scope of this article. Instead, we focus on the properties of the internal tide energy flux that radiates away from two disparate generation sites.

In Section 2, we describe the internal tides and present background information for the BBTRE (Section 2.1) and HOME (Section 2.2) regions. A direct comparison of the M_2 internal tide at each site is presented in Section 2.3. Energy flux spectra for each region are presented in Section 3. Data describing internal tide dissipation and decay are presented in Section 4. Results are discussed in Section 5.

2. Estimates of baroclinic energy flux

2.1. The Mid-Atlantic Ridge of the Brazil Basin

The Mid-Atlantic Ridge (MAR) is a prominent topographic feature of the global ocean. The MAR, and mid-ocean ridges in general, are distinguished by their large-scale tectonic structure. The topography is comprised of many fractures, which contribute to a general roughness of the bathymetry. This roughness makes the MAR an efficient generation site for internal tides. Egbert and Ray (2000, 2001) estimate that 100 GW of barotropic to baroclinic tidal conversion occurs along the MAR, representing 10% of the global internal tide production.

Direct observations relating internal tides to mixing were found during the Brazil Basin Tracer Release Experiment (BBTRE; Polzin et al., 1997; Ledwell et al., 2000; St. Laurent et al., 2001). The study was conducted in the South Atlantic in a region spanning a network of fracture zones west of the Mid-Atlantic Ridge axis. In this region (Fig. 1), topographic relief varied by up to 1 km between the crests and floors of abyssal canyons, which had typical widths of 30–50 km. Full depth measurements of fine- and microstructure velocity were made at roughly 130 station locations above the rough topography. Tidal currents in this region have been examined using the TPXO model (Egbert, 1997), and the M_2 ellipse is dominant with an amplitude of $3\,\mathrm{cm\,s^{-1}}$.

Evidence implicating tides in driving deep mixing was presented by Ledwell et al. (2000) and St. Laurent et al. (2001). These authors present vertically integrated dissipation data that are modulated over the spring-neap tidal cycle with a lag of about a day. Maximum levels of dissipation, vertically integrated to 2000 m above the bottom, reach $3\,\mathrm{mW\,m^{-2}}$. As discussed by St. Laurent et al. (2001), internal waves generated by tidal flow over the topography are the only

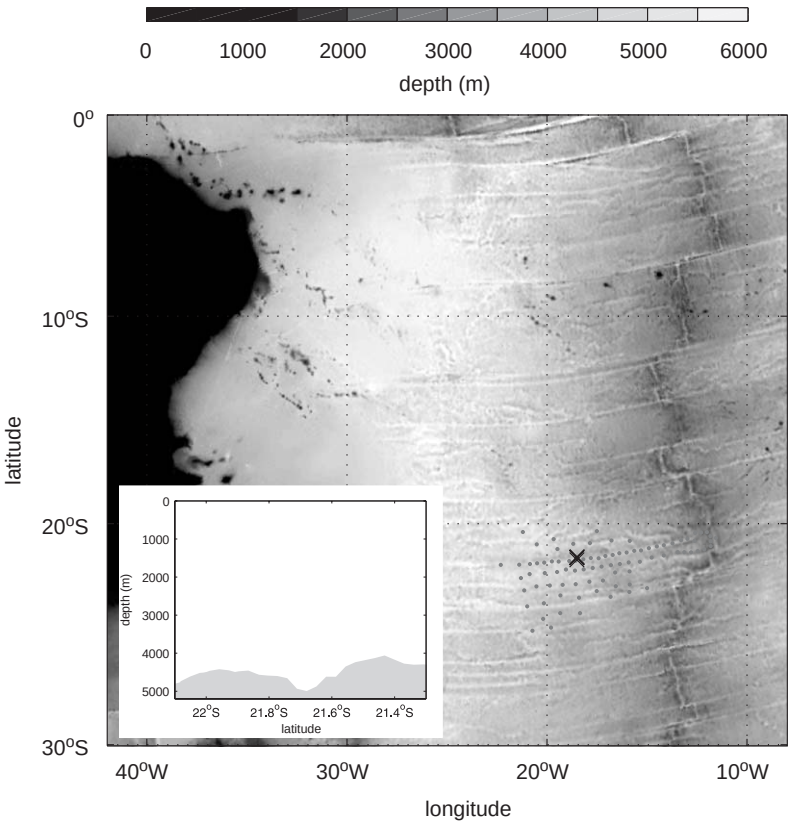

Fig. 1. Map showing the location of the Brazil Basin Tracer Release Experiment. The 1997 survey grid is shown along the flank of the MAR axis, which meanders between 12°W and 15°W. Bathymetry data from Smith and Sandwell (1997; version 8.2) were used in the figure. The location of a time series collected in 1996 at 18.5°W, 21.6°S is marked by the "x." The inset panel shows a north–south section of topography near the site of the time series.

plausible mechanism which can account for the observed energy level of the turbulence away from the bottom.

In the present analysis, we examine observations from two surveys conducted during BBTRE. The first survey consists of a time series of 17 profiles on the flank of a fracture zone canyon at 18.5°W, 21.6°S, collected over a 16-day period in 1996. The second survey consists of roughly 90 profiles spanning a nearly 1000 by 500 km region, collected over a 30-day period in 1997. The data presented here comes from the measurements of the High Resolution Profiler operated by the Woods Hole Oceanographic Institution (HRP; Schmitt et al., 1988). Data from both of these surveys are discussed by St. Laurent et al. (2001).

2.2. The Hawaiian Ridge

Like the MAR, the Hawaiian Ridge is a prominent topographic feature of the global ocean. Egbert and Ray (2000, 2001) estimate that over 20 GW of barotropic tidal energy is converted at Hawaii, much of it transferred to internal tides. Observations of internal tides were presented by Ray and Mitchum (1996, 1997), who used along-track Topex/Poseidon records to examine the surface manifestation of internal tides generated along the Hawaiian Islands. They found that both first and second baroclinic modes of the semi-diurnal (M_2) internal tides were present in the data, and that the signal of internal-tide propagation could be tracked at least 1000 km from the

Hawaiian Ridge. Ray and Mitchum (1997) assumed a two-layer stratification and estimated that 15 GW of semidiurnal internal tide energy radiates away from the Hawaiian Ridge in the first baroclinic mode. Ray and Cartwright (2001) later refined this to 6 GW using a model with more realistic stratification.

Direct observations of internal tides at the Hawaiian Ridge were made as part of the Hawaii Ocean Mixing Experiment (HOME; Pinkel et al., 2000). Both near- and far-field observational components were conducted, and fine- and microstructure measurements provided estimates of tidal energy flux and turbulent dissipation. Observations along the ridge were concentrated at a number of regions (Fig. 2), identified as having both strong (Nihoa Island, French Frigate Shoals and Kauai Channel) and weak (Necker Island) internal tide energy flux in numerical simulations (Merrifield et al., 2001). Preliminary HOME results have been reported by Rudnick et al. (2003). Here, we describe some properties of the baroclinic energy flux radiating from the Kaena Ridge of the Kauai Channel. Barotropic tides in this region are dominated by the M_2 component, with tidal velocities of $3\,\mathrm{cm\,s^{-1}}$ far from the ridge (similar to those at the BBTRE region of the MAR). Tidal speeds are much higher near the ridge, with currents of $10\,\mathrm{cm\,s^{-1}}$ in the 3000-m deep Kauai Channel increasing to $20\,\mathrm{cm\,s^{-1}}$ at water depths $<1000\,\mathrm{m}$.

We present time series observations from the 3000-m isobath of the Kauai Channel, collected in October 2000 during HOME (Kunze et al., 2004; Nash et al., 2004b). Measurements from eXpendable Current Profilers (XCPs; Sanford et al., 1993) and the Absolute Velocity Profiler (AVP; Sanford et al., 1978) were made by researchers at the University of Washington Applied Physical Laboratory. The 3000-m isobath site was occupied six times at 3-h intervals. A more comprehensive description of this survey and the treatment of finestructure data is given by Nash et al. (2004b).

2.3. Comparison of M_2 energy flux estimates

Here we examine full depth profiles of velocity and density finestructure. Specifically, we will estimate the baroclinic energy flux, $\mathbf{u}'p'$, where $\mathbf{u}'$ is the baroclinic velocity and p' is the baroclinic pressure anomaly. The baroclinic velocities are

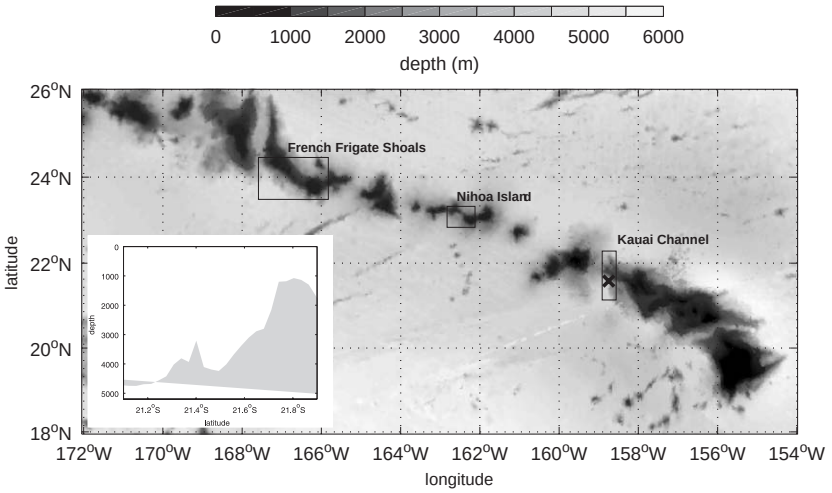

Fig. 2. Map showing several of the regions sampled during the Hawaii Ocean Mixing Experiment. French Frigate Shoals and the Kauai Channel are regions of intense baroclinic energy generation and were heavily sampled during 2000; Kauai Channel was the site of the intensive HOME nearfield experiment in 2002. Shading represents bathymetry data from Smith and Sandwell (1997; version 8.2). The location of a time series measured at the 3000-m isobath on the Kaena Ridge of the Kauai Channel (158.7°W, 21.6°N) is marked by the "x." The inset panel shows a north–south section of topography near the site of the time series.

computed directly from measured velocities: $u' = u - \overline{u}$ and $v' = v - \overline{v}$, where the barotropic components have been subtracted from each profile. The pressure anomaly was computed following the method of Kunze (Kunze et al., 2002; Nash et al., 2004c) using finestructure estimates of the buoyancy gradient N^2 and baroclinic displacement ξ,

$$p' = \rho_0 \int_z^0 N^2(z')\xi(z')\,dz' - \frac{\rho_0}{H}\int_{-H}^0\int_z^0 N^2(z')\xi(z')\,dz'dz. \quad (1)$$

The baroclinic displacements were estimated as $\xi = \zeta(\sigma;\mathbf{x},t) - \zeta(\overline{\sigma})$, where $\zeta(\sigma;\mathbf{x},t)$ are the instantaneous isopycnal depths observed at each station, and $\zeta(\overline{\sigma})$ are the averaged isopycnal depths. For the case of the BBTRE 1996 survey and the HOME 2000 survey, $\zeta(\overline{\sigma})$ was calculated using the time-mean isopycnal depths computed over the time series. For the BBTRE 1997 spatial survey, $\zeta(\overline{\sigma})$ is based on a least-square fit to each isopycnal surface of the form $\overline{\sigma}(x,y) = \varphi_{xx}x^2 + \varphi_x x + \varphi_{xy}xy + \varphi_y y + \varphi_{yy}y^2$, where the $\varphi_{(\cdot)}$ terms are the coefficients of the fit. A detailed description of this treatment of density data is given by St. Laurent et al. (2001).

Using the finestructure estimates of p' and $\mathbf{u}'$, profiles showing the instantaneous estimates $\mathbf{u}'p'$ can be computed for each of the surveys. However, only the time series data allow us to estimate the internal tide component of the baroclinic signal. Data from the BBTRE 1997 spatial survey is therefore not useful for this purpose, and will not be discussed further until Section 4.

The two time series surveys were examined using an identical analysis scheme. Vertical normal modes were computed for profiles of $\mathbf{u}'$ and p', solving the Sturm–Liouville equation numerically for the depth varying $N(z)$. The method is identical to that applied to mooring records (Alford, 2003), and results in a modal series of the form $p' \simeq \sum p_n F(z)$, where p_n are the modal amplitudes (for pressure anomaly) and $F(z)$ is the vertical structure function. A total of 25 modes were used to characterize the BBTRE profiles, while 14 were used for the HOME profiles. For each station location, a semidiurnal function of the form $\psi(t) = A\cos(\omega t) + B\sin(\omega t) + C$, was fit to the time series of normal mode amplitudes. This allows the extraction of the M_2 signal $\psi(t) - C$ with amplitude $\sqrt{A^2 + B^2}$ and phase $\phi = \arctan(A/B)$. The result is a set of profiles for baroclinic velocity and pressure anomaly that are roughly band-passed to the M_2 frequency and represented by a sum of vertical normal modes.

As described by Althaus et al. (2003) and Nash et al. (2004a), it is desirable to WKB scale the energy flux estimates as well as the depth coordinate. These transformations are given by $\hat{E}_f = (\mathbf{u}'p')\frac{N_0}{N(z)}$ and $\hat{z} = \int_z^0 \frac{N(z')}{N_0}\,dz'$, where $\hat{E}_f$ and $\hat{z}$ are the scaled energy flux and depth, respectively. For the BBTRE data, a thermocline value of $N_0 = 0.00524\,\mathrm{rad\,s^{-1}}$ was used as the reference stratification. For the HOME data, the mean stratification at the 3000-m isobath ($N_0 = 0.0029\mathrm{rad\,s^{-1}}$) was used. These scalings stretch the profiles to appear as if there was a depth constant stratification of N_0.

Fig. 3 presents profiles of the north–south component of the M_2 energy flux for the 17 profile BBTRE time series collected in 1996. These are instantaneous $v'p'$ estimates from single vertical profiles sampled at irregular intervals, so significant profile-to-profile variability is expected. In all profiles, there is a high-mode character to the energy flux. Noting the standard depth reference shown along the right-hand-side of the figure, the bottom-enhanced nature of the high-mode structure is evident. "Pulses" of $v'p'$ are most prominent in the depth range between 3000 m and the bottom, with each pulse occupying less than a 500-m vertical interval. Much weaker activity occurs in the upper 2000 m. These data suggest that the high-mode energy flux decays with a 1000–2000-m vertical scale as it radiates away from its generation site at the bottom. The mean energy flux is clearly to the north, which indicates that radiation is probably being emitted from the sloping southern side of the canyon (see Fig. 1). Energy flux levels in the mean profile are typically $1\,\mathrm{W\,m^{-2}}$, and the depth-integrated net energy flux is $1.0 \pm 0.1\,\mathrm{kW\,m^{-1}}$ in the north–northwest direction.

Fig. 4 shows profiles of the cross-ridge component of M_2 energy flux at the 3000-m isobath of

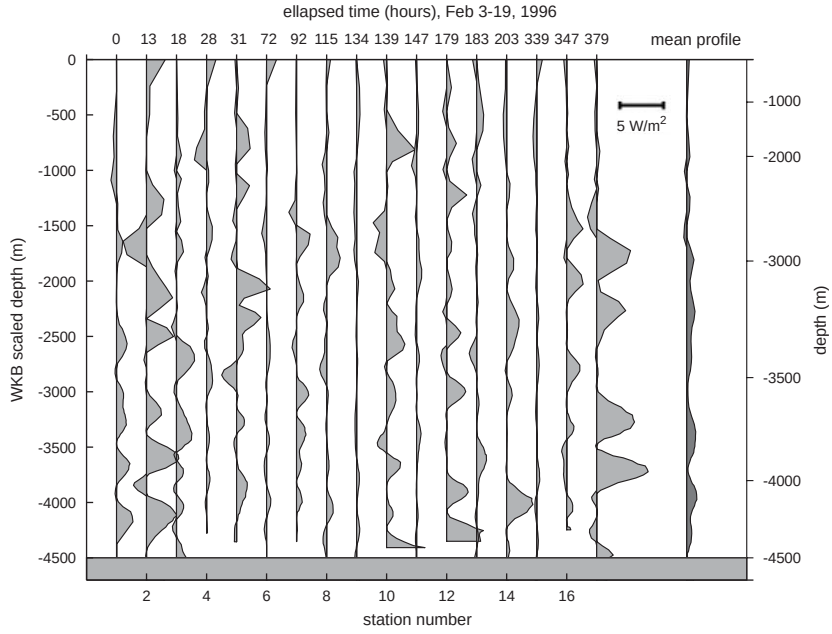

Fig. 3. A time series of instantaneous M_2 energy flux estimates $v'p'$ from 18.5°W, 21.6°S. This site is centered on a north–south slope between a 5000-m deep canyon to the south and a 4000-m deep ridge to the north. The energy flux estimates and the depth coordinate have been WKB scaled as described in the text, and the standard depth coordinate is given along the right side of the figure. Profiles were sampled at irregular intervals over a 16-day period, at times indicated along the upper axis. The mean profile is shown to the right. Energy flux plotted to the right is in the north direction.

the southern flank of the Kauai Channel. The instantaneous profiles were sampled at 3-h intervals, and a clear 6-h cycle is apparent in the time series, corresponding to the expected $\cos^2(\omega t)$ dependence of the energy flux. The baroclinic structure of energy flux is characterized by a low-mode structure, with much of the energy confined in two depth intervals, one in the upper portion of the water column and the other in the lower portion. Furthermore, each energy-flux bulge extends over a 1000-m unstretched depth scale. The mean energy flux profile for the Kauai Channel is shown to the right of Fig. 4. The flux is clearly directed south, away from the summit of the Kaena Ridge. Energy flux levels in the mean profile reach $50\,\mathrm{W\,m^{-2}}$, and the depth-integrated energy flux is $18 \pm 11\,\mathrm{kW\,m^{-1}}$.

The energy flux levels at the Kaena Ridge are $O(10)$ times larger than those measured above fracture zone topography in the Brazil Basin. This is not surprising, as the forcing of internal tides at Hawaii is stronger than at the MAR. This results from the greater topographic amplitudes (i.e., ridges $>3000\,\mathrm{m}$ high) associated with the 2000-km long Hawaii Ridge system. These intensify the barotropic currents as they are funneled through channels. In addition, the ridge topography protrudes through the thermocline, which leads to efficient baroclinic generation associated with regions of high N^2.

In addition to the disparity in energy flux magnitude, the baroclinic structure at each site is significantly different. Low modes dominate the flux at the Kaena Ridge, while high modes are clearly present at the BBTRE fracture zone site. This difference in baroclinic structure is fundamentally tied to differences in the topography at each internal tide generation site. In order to explore these details, energy flux spectra from generation models are now considered.

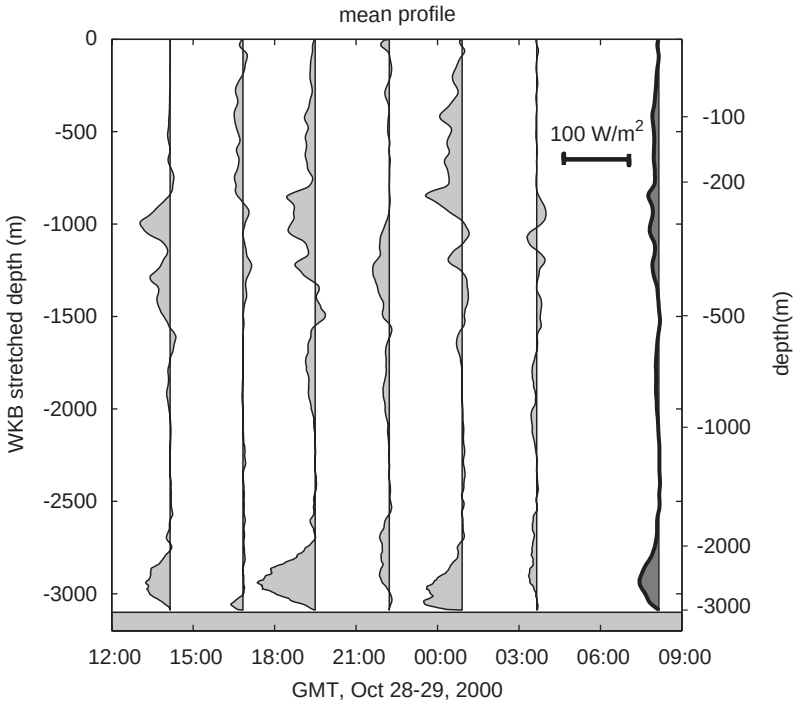

Fig. 4. Cross-ridge baroclinic energy flux density $v'p'$ radiating from Kaena Ridge, Kauai Channel. Energy flux estimates and the depth coordinate have been WKB scaled as described in the text. Instantaneous profiles from 6 occupations of the 3000-m isobath are shown. The samples were made at 3-h intervals. The mean profile is shown to the right. Energy flux plotted to the left is directed 37° west of south.

3. Energy flux spectra

An energy budget formulation for internal tides is presented by Khatiwala (2003). His formulation includes the relations between energy density, energy flux (lateral and vertical components), and the so-called barotropic to baroclinic "conversion rate." For the purpose of this article, the depth-integrated and time-averaged lateral energy flux, $\int_{-H}^{0}\langle u'p'\rangle\,\mathrm{d}z$, is regarded as equivalent to the conversion rate in the absence of dissipation. This is formally true when the tidal excursion, given by the ratio of the barotropic current amplitude to the tidal frequency, is much larger than the lateral scale of the topography. Under such conditions, the barotropic advection of baroclinic energy density is negligible. This is an excellent approximation for the internal tide generation conditions at the sites we consider in this study.

For the case of internal tides at the MAR, St. Laurent and Garrett (2002) used a linear model to examine the energy flux spectrum generated at the BBTRE site. Their calculations rely on a formulation similar to Bell (1975) and Llewellyn Smith and Young (2002), which compute energy flux based on the spectrum of bottom bathymetry. These formulations linearize the bottom boundary condition based on treating the topography as "subcritical" to internal tide generation. This refers to slope of the topography, $s = \nabla h$, being much less than the slope of the internal wave characteristics, $\alpha = \sqrt{(\omega^2 - f^2)/(N^2 - \omega^2)}$. St. Laurent and Garrett (2002) discuss in detail the applicability of the subcritical condition for MAR topography.

We present a spectral estimate for the semidiurnal internal tide energy flux at the BBTRE

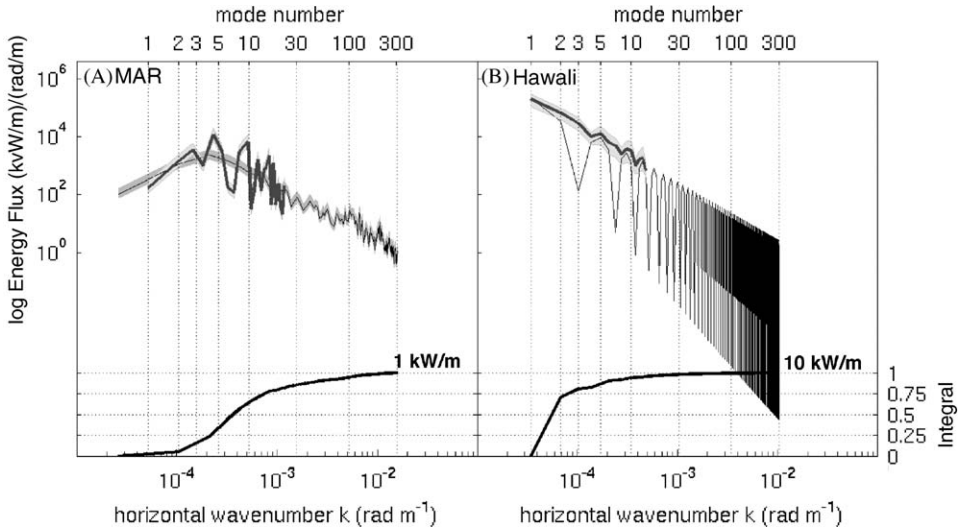

Fig. 5. (A) Spectrum for the depth-integrated average flux, $\int_{-H}^{0}\langle u'p'\rangle\,\mathrm{d}z$, for subcritical internal tide generation at a Mid-Atlantic Ridge site. Multibeam bathymetry data were used to calculate the spectrum, and the standard error confidence band is shown. The wavenumber-integrated power level is roughly $1\,\mathrm{kW\,m^{-1}}$. An observationally based estimate of the spectrum, $\int_{-H}^{0}\langle u'_n p'_n\rangle\,\mathrm{d}z$, computed from 25 normal modes, is also shown with a 95% confidence interval. (B) Spectra for depth-integrated average flux, $\int_{-H}^{0}\langle u'p'\rangle\,\mathrm{d}z$ for supercritical generation at a knife-edge ridge, used as a model for the Hawaiian Ridge. The wavenumber-integrated power level is $10\,\mathrm{kW\,m^{-1}}$. An observationally based estimate of the energy flux spectrum $\int_{-H}^{0}\langle u'_n p'_n\rangle\,\mathrm{d}z$, computed with 14 normal modes, is also shown with a 95% confidence interval. For both model estimates, the curve representing the cumulative integral of spectral power with wave number is shown.

region of the MAR in Fig. 5A. This estimate was derived from the MAR estimate of St. Laurent and Garrett (2002), who presented the time-averaged vertical component of the flux, $\langle w'p'\rangle$. Here, we have used their spectral model to calculate the horizontal energy flux, which we present in depth-integrated form, $\int_{-H}^{0}\langle u'p'\rangle\mathrm{d}z$. As shown by St. Laurent and Garrett (2002), the MAR energy flux spectrum peaks near mode 5, with modes 1–10 accounting for 60% of the total energy flux. The integrated spectrum yields an estimate of roughly $1\,\mathrm{kW\,m^{-1}}$. A spectral estimate of the energy flux was also made using the data comprising the mean profile shown in Fig. 3 (appearing on the right). This observationally based estimate is derived from the vertical-mode amplitudes and phases. The spectrum was computed as the energy flux per mode: $|u_n||p_n|\cos(\theta)\int_{-H}^{0}F^2(z)\,\mathrm{d}z$, where $\theta=\phi_u-\phi_p$ is the phase difference between u_n and p_n, and $F(z)$ is the vertical structure function of the nth mode. Confidence intervals on the spectrum were computed assuming a χ^2 cumulative density for error on the mean with 17 degrees of freedom (the number of profiles contributing to the average). The integrated power in the estimated spectrum is 2 kW/m, a factor of 2 greater than the model spectrum. However, this difference is not statistically significant considering the 95% confidence interval of the estimates. Furthermore, the model spectrum is based on multibeam bathymetry data from a slightly different region to the south of the BBTRE region, where bathymetric statistics and tidal forcing may be slightly different. Overall, there is good qualitative agreement between the shapes of the observationally and model derived-spectra, which both show peak energy levels at roughly mode 5.

Energy flux estimates have also been considered for "supercritical" topographies. In particular, St. Laurent et al. (2003) and Llewellyn Smith and Young (2003) have formulated models for calculating the energy flux generated by an abrupt tall ridge. These models are based on a knife-edge ridge; i.e., a ridge with no width along the

direction of the tidal flow. The knife-edge ridge with a height of $\frac{3}{4}$ the water depth was used to approximate the Hawaiian Ridge, and the resulting estimate of energy flux is shown in Fig. 5B. The knife-edge model spectrum is accompanied by an estimate based on the observed M_2 energy flux at the 3000-m isobath of the Kauai Channel, using the mean profile shown in Fig. 4. Wave modes for the knife-edge ridge were calculated for a water depth of 3000 m using $N = 0.004\,s^{-1}$ and $f = 5.5 \times 10^{-5}\,s^{-1}$. As shown in Fig. 5B, both the knife-edge and observationally based spectra are "red." Furthermore, the spectra show excellent correspondence in modal content. Modes 1–10 account for more than 95% of both the modeled and observed energy flux; in fact, modes 1 and 2 account for 88% of the baroclinic energy flux in both the observationally based and model estimate. The generation of low mode internal tides is clearly favored by both rough MAR topography and abrupt Hawaii-like ridges alike. However, the relative proportion of high modes to low modes is significantly higher at the Mid-Atlantic Ridge site.

The shear (u_z) of the generated internal tides is also of interest, as the Richardson number ($Ri = N^2/u_z^2$) is a crucial stability parameter for baroclinic flow. St. Laurent and Garrett (2002) examined the shear of internal tides generated at MAR topography. They computed the cumulative integral of shear variance as a function of vertical wavenumber ($u_z^2(m)$), and then defined $Ri(m) = N^2/\langle u_z^2(m)\rangle$. This provides a depth-average estimate of the shear stability of the internal tide, as opposed to an estimate of stability at any given depth. They found that, in the absence of background sheared currents, the Richardson number is large for the wavelengths that dominate the energy flux (Fig. 6A). St. Laurent and Garrett (2002) therefore conclude that shear instability is not a primary influence on the low mode energy flux generated at subcritical topography. The Richardson number for the knife-edge ridge discussed above is also considered here (Fig. 6B). As is the case for the MAR model, the Richardson number, based on mean-square shear for the knife model, is characterized by $Ri > 1$. We note that in

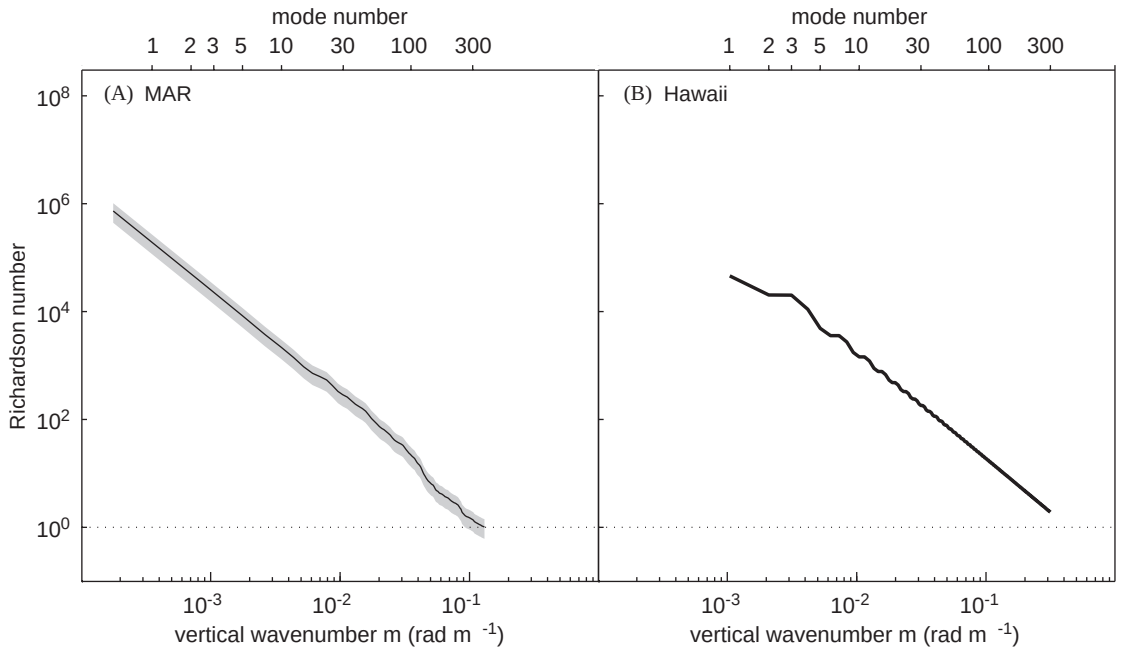

Fig. 6. The Richardson number estimated by integrating the cumulative shear variance of increasing modes for internal tides generated at (A) a mid-ocean ridge and (B) a knife-edge model approximation of the Hawaiian Ridge. In both panels, the first 300 baroclinic modes are shown. A Richardson number of unity is indicated for reference.

both cases, the Richardson numbers will drop below unity when very high modes are accounted for in the shear variance. In fact, for the case of supercritical wave generation, inviscid theories, like that of St. Laurent et al. (2003) for knife-edge generation, give infinite integrated shear variance. These extremely high modes manifest their shear in a narrow beam, as are observed at supercritical generation sites. As shown by Lien and Gregg (2001), large amounts of dissipation can occur along the path of the beam. However, it seems unlikely that the energy flux carried by the lowest modes is influenced by the low Richardson numbers associated with beam-like structures.

Subtle but important differences in *Ri* are evident between the HOME and BBTRE data shown in Fig. 6. Despite the low-mode internal tide being 10 times more energetic at the Hawaiian Ridge, its energy flux spectrum is redder so that the energy at high-wavenumbers is less than the MAR. This is illustrated by the fact that the spectral estimate of *Ri* from modes 1–300 is a factor of 3 larger at the Hawaiian Ridge than at the MAR. Hence, internal tides with 10-m vertical wavelength at the MAR may be susceptible to shear instability, while those same wavelengths at the HOME site may be stable, simply due to differences in the shape of the energy spectrum. Since turbulent overturns at the Hawaiian Ridge are observed to be many hundred meters in vertical extent (Slinn and Levine, 2003; Klymak et al., 2004), it is possible that the mechanism for dissipation at HOME is not the direct generation at M_2 frequencies, as was suspected at the MAR. Instead, different mechanisms may be in play at the Hawaiian Ridge; parametric subharmonic instability has been suggested as one such possibility to move variance directly from stable M_2 waves to high wavenumber, lower-frequency motions that may be susceptible to shear instability (i.e., MacKinnon and Winters, 2003).

We again emphasize that the spectral estimate of *Ri* is a depth-averaged quantity. It underestimates the amount of localized shear when a superposition of waves constructively interfere or are spatially phased-locked and form beam-like structures. This is likely near the Hawaiian Ridge (where phase-locking is observed), but has not been quantified.

4. Internal tide dissipation and decay

Direct measurements of velocity microstructure taken during BBTRE and HOME allow us to examine profiles of the energy dissipation rate (ε) at each internal tide generation site. Average profiles are shown in Fig. 7. Dissipation rate data from BBTRE have been previously discussed by Ledwell et al. (2000) and St. Laurent et al. (2001), and dissipation rate estimates from HOME are described in Rudnick et al. (2003) and Klymak et al. (2004). Despite the fact that energy flux levels are stronger at the Hawaiian Ridge, the average dissipation profiles from HOME and BBTRE are

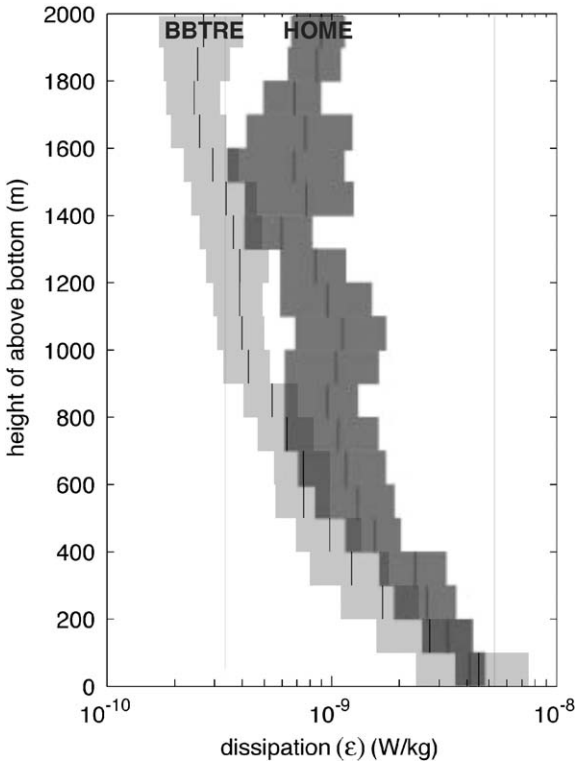

Fig. 7. Profiles of the turbulent dissipation rate ε from BBTRE and HOME observations. In both cases, dissipation rates were averaged into 100-m vertical bins and smoothed by a 3-bin running average. The 95% confidence band is shown for all estimates. The BBTRE profile is an average of 129 profiles from surveys in 1996 and 1997 spanning a 1000 km by 500 km region. The HOME profile is an average over 70 profiles spanning sites along the 3000-m isobath of the Hawaiian Ridge from French Frigate Shoals to Kauai Channel.

similar in both magnitude and depth dependence up to heights of 800 m above the bottom. At each site, the dissipation rate is maximum just above the topography, and the profiles decay with height with an e-fold scale of roughly 300–500 m. Above 800 m, the average profile from the Hawaiian Ridge shows dissipation values significantly larger than those observed at the MAR. We note that this difference is partially due to the buoyancy scaling of ε, as discussed by Polzin et al. (1995). Heights above 800 m at the MAR extend into the weakly stratified abyssal interior, while considerably more stratification exists at these heights along the Hawaiian Ridge.

Simultaneous observations of fine- and microstructure made during BBTRE and HOME permit estimation of a spatial decay scale for the radiated internal tides. For each profile, the depth-integrated energy flux was normalized by the depth-integrated turbulent energy dissipation to yield a "decay length" of the radiated tide, given by

$$L_\varepsilon \simeq \frac{\int \langle \mathbf{u}' p' \rangle \, \mathrm{d}z}{\int \rho \varepsilon \, \mathrm{d}z}, \tag{2}$$

as shown in Fig. 8. In (2), the vertical integrals were computed over the depth range between 100 m and the bottom (i.e., neglecting the surface-influenced 100 m). This decay scale represents the e-folding scale for an internal wave assuming the dissipation rate is constant along the path of propagation and negligible radial dispersion. This is obviously an approximate assumption, as the dissipation rate clearly varies spatially. Most likely, L_ε is an underestimate of the decay scale, since ε decays with distance from its energy source (Klymak et al., 2004). Nevertheless, the estimates presented here provide an order of magnitude scale for the decay of internal tide energy as it radiates away from regions of generation. Decay scales at the MAR (panel a) are less than those observed at the Hawaiian Ridge (panel b). The mean decay scale for the BBTRE data is 230 ± 70 km, and 750 ± 240 km for the HOME data. The difference in these mean estimates is significant at the 95% confidence level. Additionally, the minimum and maximum L_ε for BBTRE are 77 and 460 km, while these are 150 and 2200 km for HOME. The O(100)km decay scale for the MAR has not been previously documented. However, the scale is consistent with the abrupt decrease in

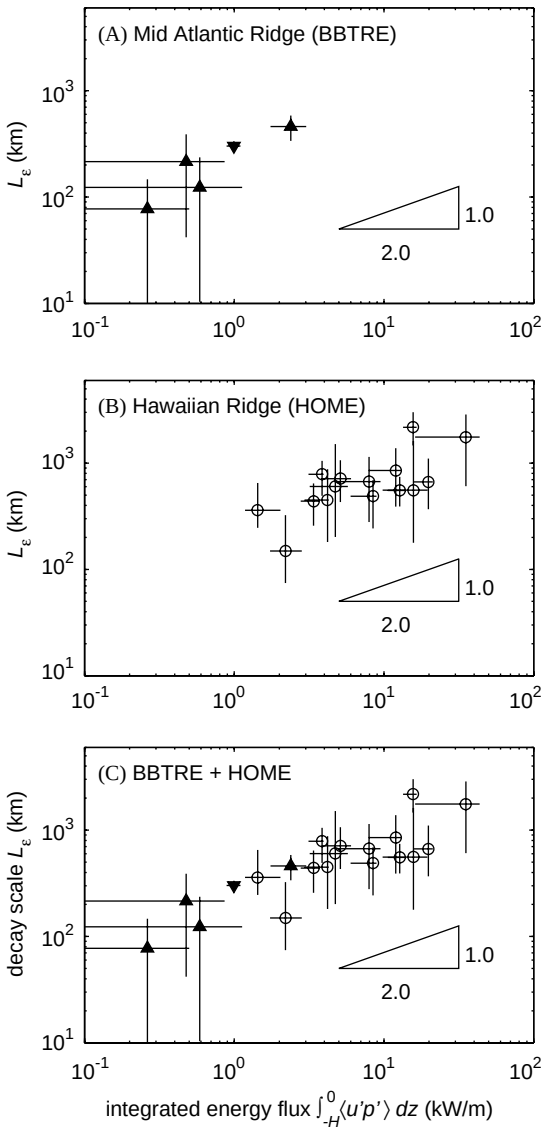

Fig. 8. Spatial decay scale L_ε as a function of depth-integrated energy flux. (A) Estimates from BBTRE 1996 (downward triangle) and BBTRE 1997 (upward triangles). Roughly 15 profiles were averaged for each estimate, and 95% confidence intervals are shown. (B) Estimates from the 3000-m isobath at the Hawaiian Ridge; each symbol represents a >5 profile average from each of 16 different station occupations. (C) Combined estimates from BBTRE and HOME. Error bars represent 95% bootstrap confidence intervals.

turbulence levels away from the rough topography of the MAR (Polzin et al., 1997). The $O(1000)$km decay scales estimated at Hawaii are consistent with the correlation scales documented by Ray and Mitchum (1996) for the lowest mode internal tide radiated from the Hawaiian Ridge, although some of the decay perceived from the satellite measurements may result from loss of coherence of the M_2 tide as it passes through mesoscale features (Rainville, pers. comm.).

Fig. 8 shows that the largest decay scales are associated with the largest energy fluxes. We associate large energy flux with abundant low mode energy, which is able to radiate over large distances. We postulate the presence of dissipative high modes is only weakly related to the amount of low mode energy flux generation, so that dissipation occurs in higher proportion at sites of weak generation.

5. Discussion

We have presented estimates of baroclinic energy flux from two very different internal tide generation regions. The Mid-Atlantic Ridge site studied as part of BBTRE provides an example of internal tide generation by deep rough topography. In contrast, the Hawaiian Ridge sites studied during HOME provide examples of internal tide generation at abrupt high-amplitude topography. These two generation-regions provide examples from significantly different baroclinic wave forcing regimes of the deep ocean. As discussed by St. Laurent and Garrett (2002), the MAR is characterized by subcritical slopes, in that the radiated path of the internal tide is steeper than the large-scale slope of the bottom topography. This contrasts the Hawaiian Ridge, where internal tides propagate along ray paths less steep than the bottom. Nash et al. (2004b) show that the observed beams of M_2 energy at HOME are consistent with localized generation over the steep supercritical flanks (i.e., regions of strong barotropically induced vertical displacements; Baines, 1982) and subsequent propagation along internal tide ray paths. The beam-like nature near the ridge crest evolves into a more modal character by the 3000-m isobath, the site of dissipation measurements presented here.

Estimates of energy flux from the BBTRE site show considerable high mode character (Fig. 3). This is consistent with the modeled spectrum of energy flux (Fig. 5A), which shows an energy flux maximum at mode 5. Such high mode generation is clearly linked to the scales of the dominant fracture zone topography. The horizontal wavelength of the mode-5 M_2 internal tide is 30 km, roughly matching the characteristic wavelength of the canyon-crest system. Finer topographic scales are present in the form of abyssal hills in the canyons and on the ridge crests. These lead directly to high wavenumber generation, as discussed by Polzin (2004).

In contrast, the energy flux from the Hawaiian Ridge originates as low modes because of the topographical scale. The horizontal span of the Kaena Ridge appears to preferentially favor generation into modes 1 and 2, which produces beams along the summit of the ridge (Nash et al., 2004b) that quickly evolve into low modes by the 3000-m isobath (Fig. 4). As shown by the spectral estimate (Fig. 5B), the energy flux spectrum is "red," with most of the energy in modes 1 and 2. St. Laurent et al. (2003) suggest that low-mode energy flux is a general feature of internal tides generated by all abrupt tall ridges in the ocean. While high wavenumbers are generated in order to form the beam-like baroclinic structure, they represent only a small fraction of the energy flux and likely dissipate more quickly than their low-mode counterparts.

Despite the considerable differences in the radiated energy flux at these sites, the rate of energy dissipation of the internal tide is similar. Maximum dissipation levels of $\varepsilon = 10^{-9} - 10^{-8}\,\mathrm{W\,kg^{-1}}$ occur along the bottom in both regions (Fig. 7). Additionally, the height dependence of the dissipation profiles are of similar scale, particular within 800 m of the bottom. Decay scales, as estimated by normalizing the integrated energy flux by the integrated dissipation, range from $O(100)$km to $O(1000)$km. The mean estimate of L_ε is a factor of 3 less for the MAR. This is consistent with the higher-mode content of the MAR energy flux, as high modes are

more likely to dissipate close to their generation site (St. Laurent and Garrett, 2002).

In conclusion, the significant differences in internal tide generation at the MAR and Hawaiian Ridge do not lead to significant differences in the magnitude of the turbulent energy dissipation. If this result is general, there are interesting implications concerning the underlying physics of dissipation. It would seem that the overall level of dissipation is not sensitive to the total energy flux. Instead, we propose that the dissipation level scales only with the energy available in the high modes. A rough analysis follows from considering the energy flux in modes >10 for each site. For the MAR site, modes >10 comprise 40% of the 1–2 $\mathrm{kW\,m^{-1}}$ of depth integrated flux (Fig. 5A), thus accounting for 0.4–0.8 $\mathrm{kW\,m^{-1}}$. Similarly, modes >10 at the Hawaiian Ridge comprise 5% of the 10 $\mathrm{kW\ m^{-1}}$ of integrated flux (Fig. 5B), accounting for 0.5 $\mathrm{kW\,m^{-1}}$. Thus, while the overall energy flux levels differ, the high-mode energy level is comparable at the two sites. The high-mode energy density may thus provide a better scaling for the turbulent energy dissipation rate, as suggested by Klymak et al. (2004).

As argued by St. Laurent and Garrett (2002), energy flux in high modes will dissipate locally, as their group speed is very small and their wave–wave interaction rates are large. This leaves the low modes to radiate their energy away, apparently to considerable distances. Where and how the low mode energy dissipates remains an open question.

Acknowledgements

Data presented in this report were collected by a number of investigators. We thank Tom Sanford, Eric Kunze and Craig Lee for their efforts in the collection and interpretation of Hawaii Ocean Mixing Experiment data presented in this report. Additionally, we are grateful to John Toole, Ray Schmitt, and Kurt Polzin for their efforts associated with the BBTRE program and data. We thank Eric Kunze, Jen Mackinnon, Rob Pinkel, and two anonymous reviewers for their helpful comments. This research has been funded by grants from NSF and ONR.

References

Alford, M.H., 2003. Redistribution of energy available for ocean mixing by long-range internal-wave propagation. Nature 423, 159–163.

Althaus, A.M., Kunze, E., Sanford, T.B., 2003. Internal tide radiation from Mendocino Escarpment. Journal of Physical Oceanography 33, 1510–1527.

Baines, P.G., 1973. The generation of internal tides by flat-bump topography. Deep-Sea Research 20, 179–205.

Baines, P.G., 1982. On internal tide generation models. Deep-Sea Research 29, 307–338.

Balmforth, N.J., Ierley, G.R., Young, W.R., 2002. Tidal conversion by subcritical topography. Journal of Physical Oceanography 32, 2900–2914.

Bell, T.H., 1975. Lee waves in stratified flows with simple harmonic time dependence. Journal of Fluid Mechanics 67, 705–722.

Cox, C.S., Sandstrom, H., 1962. Coupling of surface and internal waves in water of variable depth. Journal of the Oceanographic Society of Japan, 20th Anniversary Volume, pp. 499–513.

Egbert, G.D., 1997. Tidal data inversion: interpolation and inference. Progress in Oceanography 40, 81–108.

Egbert, G.D., Ray, R.D., 2000. Significant dissipation of tidal energy in the deep ocean inferred from satellite altimeter data. Nature 405, 775–778.

Egbert, G.D., Ray, R.D., 2001. Estimates of M2 tidal energy dissipation from TOPEX/POSEIDON altimeter data. Journal of Geophysical Research 106, 22475–22502.

Egbert, G.D., Bennett, A.F., Foreman, M.G.G., 1994. TOPEX/POSEIDON tides estimated using a global inverse model. Journal of Geophysical Research 99, 24821–24852.

Hibiya, T., 1986. Generation mechanism of internal waves by tidal flow over a sill. Journal of Geophysical Research 91, 7696–7708.

Khatiwala, S., 2003. Generation of internal tides in an ocean of finite depth: analytical and numerical calculations. Deep-Sea Research 50, 3–21.

Klymak, J.M., Moum, J.N., Nash, J.D., Kunze, E., Girton, J.B., Carter, G.S., Lee, C.M., Sanford, T.B., Gregg, M.C., 2004. An estimate of energy lost to turbulence at the Hawaiian Ridge. Journal of Physical Oceanography, submitted.

Kunze, E., Rosenfeld, L.K., Carter, G.S., Gregg, M.C., 2002. Internal waves in the Monterey submarine canyon. Journal of Physical Oceanography 32, 1890–1913.

Kunze, E., Sanford, T.B., Lee, C.M., Nash, J.D., Merrifield, M.A., Holloway, P., 2004. A survey of internal tides and turbulence along the Hawaiian Ridge with model comparisons. Journal of Physical Oceanography, in preparation.

Ledwell, J.R., Montgomery, E.T., Polzin, K.L., St. Laurent, L.C., Schmitt, R.W., Toole, J.M., 2000. Mixing over rough topography in the Brazil Basin. Nature 403, 179–182.

Legg, S., 2004a. Internal tides generated on a corrugated continental slope. Part I: cross-slope barotropic forcing. Journal of Physical Oceanography 34, 156–173.

Legg, S., 2004b. Internal tides generated on a corrugated continental slope. Part II: along slope barotropic forcing. Journal of Physical Oceanography 34, 1824–1838.

Legg, S., Adcroft, A., 2003. Internal wave breaking at concave and convex continental slopes. Journal of Physical Oceanography 33, 2224–2246.

Lien, R.-C., Gregg, M.C., 2001. Observations of turbulence in a tidal beam and across a coastal ridge. Journal of Geophysical Research 106, 4575–4592.

Llewellyn Smith, S.G., Young, W.R., 2002. Conversion of the barotropic tide. Journal of Physical Oceanography 32, 1554–1566.

Llewellyn Smith, S.G., Young, W.R., 2003. Tidal conversion at a very steep ridge. Journal of Fluid Mechanics 495, 175–191.

MacKinnon, J.A., Winters, K.B., 2003. Spectral evolution of bottom-forced internal waves. Proceedings of the 13th 'Aha Huliko' a Hawaiian Winter Workshop, pp. 73–83.

Merrifield, M.A., Holloway, P.E., Shaun Johnston, T.M., 2001. Internal tide generation at the Hawaiian Ridge. Geophysical Research Letters 28, 559–562.

Nash, J.D., Kunze, E., Toole, J.M., Schmitt, R.W., 2004a. Internal tide reflection and turbulent mixing on the continental slope. Journal of Physical Oceanography 34 (5), 1117–1134.

Nash, J.D., Kunze, E., Sanford, T.B., Lee, C.M., 2004b. Structure of the baroclinic tide generated at a ridge. Journal of Physical Oceanography, submitted.

Nash, J.D., Alford, M.H., Kunze, E., 2004c. On estimating internal-wave energy fluxes in the ocean. Journal of Atmospheric Oceanic Technology, submitted.

Petrelis, F., Llewellyn Smith, S.G., Young, W.R., 2004. Tidal conversion at a submarine ridge. Journal of Physical Oceanography, in press.

Pinkel, R., Munk, W., Worcester, P., et al., 2000. Ocean mixing studied near Hawaiian Ridge. EOS Transactions of the American Geophysical Union 81, pp. 545,553.

Polzin, K.L., 2004. Idealized solutions for the energy balance of the finescale internal wave field. Journal of Physical Oceanography 34, 231–246 doi:10.1175/1520-0485(2004)034.

Polzin, K.L., Toole, J.M., Schmitt, R.W., 1995. Finescale parameterizations of turbulent dissipation. Journal of Physical Oceanography 25, 306–328.

Polzin, K.L., Toole, J.M., Ledwell, J.R., Schmitt, R.W., 1997. Spatial variability of turbulent mixing in the abyssal ocean. Science 276, 93–96.

Ray, R.D., Cartwright, D.E., 2001. Estimates of internal tide energy fluxes from Topex/Poseidon altimetry: Central North Pacific. Geophysical Research Letters 28, 1259–1263.

Ray, R., Mitchum, G.T., 1996. Surface manifestation of internal tides generated near Hawaii. Geophysical Research Letters 23, 2101–2104.

Ray, R., Mitchum, G.T., 1997. Surface manifestation of internal tides in the deep ocean: observations from altimetry and island gauges. Progress in Oceanography 40, 135–162.

Rudnick, D.L., Boyd, T.J., Brainard, R.E., et al., 2003. From tides to mixing along the Hawaiian Ridge. Science 301, 355–357.

Sanford, T.B., Drever, R.G., Dunlap, J.H., 1978. A velocity profiler based on the principles of geomagnetic induction. Deep-Sea Research 25, 183–210.

Sanford, T.B., D'Asaro, E.A., Kunze, E.L., Dunlap, J.H., Drever, R.G., Kennelly, M.A., Prater, M.D. Horgan, M.S., 1993. An XCP user's guide and reference manual. Applied Physics Laboratory Technical Report. APL-UW TR9309, University of Washington, Seattle, WA.

Schmitt, R.W., Toole, J.M., Koehler, R.L., Mellinger, E.C., Doherty, K.W., 1988. The development of a fine- and microstructure profiler. Journal of Atmospheric and Oceanic Technology 5, 484–500.

Slinn, D.N., Levine, M.D., 2003. Modeling internal tides and mixing over ocean ridges. Proceedings of the 13th 'Aha Huliko' a Hawaiian Winter Workshop, pp. 59–68.

St. Laurent, L.C., Garrett, C., 2002. The role of internal tides in mixing the deep ocean. Journal of Physical Oceanography 32, 2882–2899.

St. Laurent, L.C., Toole, J.M., Schmitt, R.W., 2001. Buoyancy forcing by turbulence above rough topography in the abyssal Brazil Basin. Journal of Physical Oceanography 31, 3476–3495.

St. Laurent, L.C., Simmons, H.L., Jayne, S.R., 2002. Estimating tidally driven mixing in the deep ocean. Geophysical Research Letters 29, 2106 doi:10.1029/2002GL015633.

St. Laurent, L., Stringer, S., Garrett, C., Perrault-Joncas, D., 2003. The generation of internal tides at abrupt topography. Deep-Sea Research 50, 987–1003.